Catalytic Bias and Redox-Driven Inactivation of the Group B FeFe Hydrogenase CpIII

Andrea Fasano, Aurore Jacq-Bailly, Jeremy Wozniak, Vincent Fourmond, Christophe Léger

This is the author version of A. Fasano *et al*, ACS Cat. 2024 doi: 10.1021/acscatal.4c01352

Catalytic bias and redox-driven inactivation of the group B FeFe hydrogenase CpIII

Andrea Fasano, Aurore Jacq-Bailly, Jeremy Wozniak, Vincent Fourmond, Christophe Léger*

Laboratoire de Bioénergétique et Ingénierie des Protéines, CNRS, Aix Marseille Université, Marseille, France.

* leger@imm.cnrs.fr

Abstract

The biodiversity of hydrogenases, the enzymes that oxidize and produce H_2, is only just beginning to be explored. Here we use direct electrochemistry to characterize two enzymes from a subgroup of group B FeFe hydrogenases, defined by the presence of three adjacent cysteine residues near the active site: the third FeFe hydrogenase from *Clostridium pasteurianum* (CpIII) and the second from *Megasphaera elsdenii* (MeII). To examine the functional role of the unusual TSCCCP motif, which is replaced with TSCCP in group A hydrogenases, we also produced a CpIII variant where the supernumerary cysteine is deleted. CpIII and MeII inactivate under oxidative conditions in a manner that is distinct from all other previously characterized hydrogenases from group A. Our results suggest that the supernumerary cysteine allows the previously observed sulfide-independent formation of the H_{inact} state in these enzymes. We also evidence a second reversible, oxidative inactivation process that is independent of the supernumerary cysteine. Because of their inactivation under oxidative conditions, these enzymes are inefficient H_2 oxidation catalysts, but their active site itself is not tuned to make them more active in one particular direction.

Introduction

Hydrogenases, the enzymes that oxidize and produce hydrogen, come in three different flavors — FeFe hydrogenases, NiFe hydrogenases, and Fe hydrogenases — named after the metal content of their active sites. Nitrogenases also produce H_2 as a byproduct of nitrogen reduction.

The active site "H-cluster" of FeFe hydrogenases (leftmost in figure 1A) consists of a dinuclear Fe_2 cluster that is coordinated by 3 carbonyl and 2 cyanide ligands, an amine-dithiolate ligand (adt, or azadithiolate), and a cysteine thiolate that covalently attaches the dinuclear site to a [4Fe4S] cluster. The Fe ion that is remote from the cubane is referred to as "distal", or Fe_d. The diatomic ligands can be detected by FTIR spectroscopy, and their vibrations have been used to identify various states of the H-cluster, including catalytic intermediates[1–5].

In the catalytic cycle, H_2 binds to the apical, empty coordination site on Fe_d when the active site is in the H_{ox} 'resting' state ($[4Fe4S]^{2+}Fe^{II}Fe^{I}$). H_2 is split into a hydride and a proton which is transferred to the nitrogen of the amine ligand. The H-cluster is connected to the solvent by a series of residues that mediate long range proton transfer (a conserved cysteine, C299 in figure 1A, is in many hydrogenase the 1st proton acceptor along the chain[3,6]), elusive gas channels that guide the diffusion

of small molecules, and, in some enzymes, accessory FeS clusters that are used to mediate electron transfer.

FeFe hydrogenases are present in many microorganisms, both prokaryotes and eukaryotes, and are very diverse[7]. The environment of the active site is characterized by three sequence signatures or "motifs" (written hereafter using the PROSITE format,[8] where brackets include the residues occurring at a single position in the set of sequences, and “x” means “any aminoacid”): P1, [FILT][ST][SCM]C[CS]P[AGSMIV][FWY], P2, [FILV][MGTV]PCxxK[DKQRS]x[EV], and P3, ExMxCxxGCxxG[AGP])[9]. Greening *et al.* have recently defined three phylogenetic groups: A (prototypical and bifurcating), B (qualified as "ancestral" in their work for reasons that have not been developed) and C (putative sensory)[10]; Calusinska *et al.* also defined a group D of putative hydrogenases[11]. An earlier, structural classification is based on the number of accessory FeS clusters: zero (M1), two (M2), or four clusters (M3), as exemplified by the three group A1 enzymes from *Chlamydomonas reinhardtii* (Cr HydA1), *Desulfovibrio desulfuricans* and *Clostridium pasteurianum* (CpI), respectively[12]. These three prototypical enzymes have been the focus of most of the biophysical studies of FeFe hydrogenases, but atypical hydrogenases have recently been characterized and unexpected features have emerged[13].

For example, the group A "CbA5H" FeFe hydrogenase from *C. beijerinckii* (Cb) is protected from oxygen damage by the binding to the distal Fe ion of the conserved cysteine that is the first proton relay; this binding can occur because non-conserved residues that are remote from the active site make the protein loop that bears the cysteine residue more flexible than in other hydrogenases[4,14,15]. In the group D FeFe hydrogenase from *Thermoanaerobacter mathranii*, protons are transferred along a pathway that is entirely distinct from that of prototypical hydrogenases[16,17], and catalysis is 'irreversible', that is H_2 oxidation and production only occur at the price of a large thermodynamic driving force[18,19].

Related to the above comment about (ir)reversible catalysis, another catalytic property that has attracted much interest is the 'catalytic bias', defined as the ratio of the maximal rates in the two directions of the reaction (H_2 oxidation and production)[20]. Three homologous FeFe hydrogenases from *C. pasteurianum* illustrate how the protein that embeds the active site can tune the enzyme's catalytic bias by orders of magnitude: the enzyme CpI is equally efficient in the oxidative and reductive directions, whereas the homologous enzymes CpII (group A) and CpIII (group B) are strongly biased for oxidative and reductive catalysis, respectively[5].

In 2019, the fact that CpIII is nearly inactive for H_2 oxidation in solution assays was related by Peters and coworkers to the ease with which the active site is oxidized above its normal resting state H_{ox}. The overoxidized "H_{ox+1}" state is reminiscent of the "H_{inact}" state observed in other FeFe hydrogenases, but it is observed in CpIII under less oxidizing conditions. These unique properties were assigned to the more hydrophobic environment of the H-cluster in CpIII, compared to CpI and CpII, which would destabilize the H_{ox} state and thus favor proton reduction[5].

At that time, the implication of the observation of the H_{inact} state in CpIII was not discussed. Only shortly after did it become clear that this state, which is also observed when exogenous sulfide binds to the distal Fe in prototypical FeFe hydrogenases[21,22], reveals the binding to the distal Fe of the intrinsic sulfide of a cysteine residue, as occurs in the enzyme from *C. beijerinckii*[14]. The hypothesis that this also occurs in CpIII is particularly appealing because the environment of its H cluster is cysteine rich: the P1 motif, most comonly xTSCCPxx, is present as ITSCCCPMW. This peculiar TSCCCP

motif defines the FeFe hydrogenase subgroups 'M2a' and 'B2' according to Meyer[12] and Calusinska *et al.*[11], respectively. Its functional significance is discussed in this paper, where we examine the catalytic properties of two M2a/B2 enzymes: CpIII (WP_003447632.1) and *Megasphaera elsdenii* II ("MeII", WP_169013299.1, distinct from the enzyme studied in refs [23,24]), and a CpIII site directed mutant where the supernumerary cysteine is deleted.

Results

Structural considerations

We examined 274 group B sequences listed on the hydrogenase database website[25] (we removed WP_025640716.1, which lacks the P1 motif, and included the CpIII and MeII sequences). In this group, the xTSCCPxx motif is the most common version of P1 (134 occurrences), followed by TSCCCPxx (75 occurrences). The latter is specific to group B: none of the 955 hydrogenase sequences classified as group A or C listed on the hydrogenase database included a CCC triad.

In all sequences in group B, the first run of four cysteines, which is Cx2Cx2Cx3C in prototypical hydrogenases (blue and green dots in SI figure S7), is highly variable, with a consequence on the environment of the accessory [4Fe4S]Cys_4 cluster that is distal from the active site (SI figure S9), as mentioned before[11,12].

SI figure S8 compares the alphafold[26] model structure of the WT CpIII and that of the hydrogenase from *D. desulfuricans* (pdf 1HFE[27]). Both are classified as M2 (because they embed two accessory FeS clusters), one of which is exposed at the surface of the protein and is the entry point for electrons in the enzyme, when it interacts with redox partners or with an electrode. The enzyme from *D. desulfuricans* has been extensively studied using protein film electrochemistry (see e.g. ref [21]), and it is not a surprise that the CpIII enzyme can also transfer electrons to an electrode (see below). The overall fold is the same in CpIII and *D. desulfuricans* hydrogenase, except that the former has a 70-residue N-terminal additional domain.

Figure 1A focuses on the proton transfer pathway. It shows the structure of CpIII aligned on the structure of CpI (pdb 6N59[5]). The CpI residues are shown in gray. A cluster of red balls indicate the positions of a water molecule that is seen in many structures of group A1 FeFe hydrogenases (see the list in Table S1 in ref [22]). Proton transfer from the active site to the solvent involves C299, this water molecule (HOH 612 in pdb 3C8Y, absent in pdb 6N59), E279, S319, E282 and R286[3,6] (black dots in SI figure S7). According to a Clustalω alignment[28] of 204 group A1 sequences, this proton transfer chain is very conserved (Table 1): the first glutamate is substituted in only 3 sequences, the second glutamate is also substituted in 3 sequences, the serine is substituted in only one sequence, and the arginine is substituted (most often with lysine) in only 22 sequences. This series of residues is more variable in group B (second row in Table 1): the first glutamate is present in all but one group B sequences (WP_013255832.1) out of 274, but the second glutamate is replaced with D or H in about 40 group B sequences (none of which includes the CCC triad) ; the serine is absent from about 30 other group B sequences, and the arginine is rarely present. This shows that there are many small variations on the typical proton transfer pathway in the hydrogenases from group B.

Residue in CpI	C299	E279	S319	E282	R286	SCCP motif
group A1	C 97.5% else T, W, S, A or F	E 98.5% else I or D	S 99.5% else A	98.5% else I, D or P	R 90% K 8% else H,F,M	SCCP 89% SCSP 4% (*)
group B	C 100%	E 99.6% (*)	S 89% T 1.7% P 8% else L, Q	E 87.8% D 9.5% H 2.8% else L, Y, M, K, I	R 15% H 10% K 10% N 7% (*)(**)	SCCP 66% SCSP 0% MCCP 1.5% SCCCP 26% (*)

Table 1. The frequencies of the proton transfer pathway residues and the nature of the TSC fragment in 204 sequences of group A1 hydrogenases and 274 sequences of group B hydrogenases available on the hydrogenase database when this paper was submitted. (*) The total is not 100% : other options are not listed. (**) The alignment is probably not very reliable in this part of the group B sequences.

The positions of the CpIII residues C223 (equivalent to CpI C300, which coordinates the cubane of the H-cluster), C222, C221, E202, S242, E205 and H209 (which take the same positions as the residues of the proton transfer pathway in group A hydrogenases) are shown in green in figure 1A. The proton transfer pathway is the same in CpI and CpIII, except that a histidine in CpIII replaces R286, and the sulfur of the supernumerary cysteine (C221) is very close to the position of the conserved water molecule. This suggests that C221 mediates proton transfer from C222 to E202 in CpIII.
A methionine, which replaces the 1st of the three cysteines in a small number of group B sequences (table 1), may play the same role. The Alphafold model of MeII (not shown) is similar to that of CpIII, but the putative proton transfer pathway is less well defined; it would involve C183, C182, E163, E166 but the serine position (S319 in CpI) is occupied by P203 according to the alignment, and the distal arginine by N170 (black dots in SI figure S7).

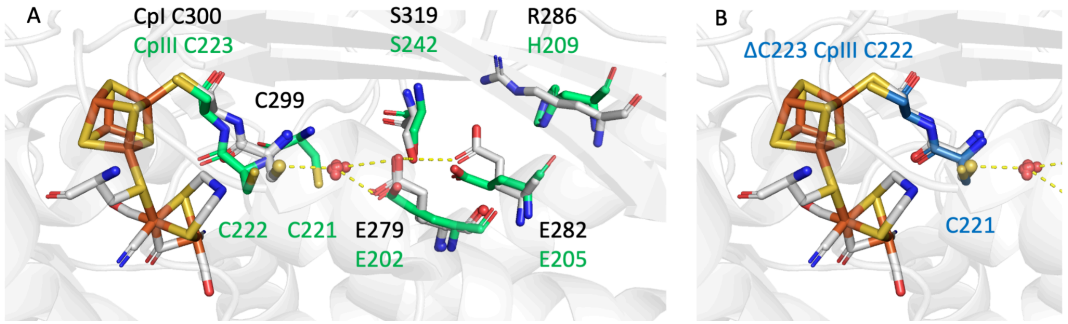

Figure 1. The model structure of CpIII (A) and the ΔC variant (B), aligned on the structure of CpI. Gray sticks indicate the positions of selected CpI residues (light gray, pdb 6N59[5]), the red spheres show the positions of a conserved water molecule in various structures of group A1 FeFe hydrogenases (see the list in Table S1 in ref [22]). Green sticks show the CCC triad of CpIII and four other residues that are probably involved in proton transfer (AlphaFold model). B: The position of the CC diad in the model structure of the ΔC mutant of CpIII (blue), compared to the position of the CpI residues (gray). SI figure S8 compares the overall folds of CpIII and *D. desulfuricans* hydrogenase (both of type M2), and figure S8 focuses on the environment of the accessory FeS clusters

Figure 1B shows the Alphafold model of the structure of the ΔC223 CpIII mutant, where one of the three adjacent cysteines is removed from the sequence: the positions of the two cysteines of the TSCCP motif (blue) match those of CpI (gray), suggesting that the environment of the active site in the ΔC CpIII mutant is very similar to that of group A hydrogenases.

Electrochemistry

We examined the functional properties of CpIII and MeII using protein film electrochemistry[29–32]. In these experiments, a small amount of enzyme is adsorbed onto, and exchanges directly electrons with a rotating disc electrode, which is spun at a high rate to prevent the depletion of H_2 near the electrode. The electrode potential is set to a value that is positive or negative with respect to the H^+/H_2 Nernst potential to drive H_2 oxidation or production, respectively, and the activity is measured as a current that is proportional to the turnover frequency of the enzyme and to the electroactive coverage. The latter is unknown, so that the actual value of the turnover frequency cannot be deduced from the value of the current, but much information can be gained by examining the relative change in current when the electrode potential is changed stepwise (in chronoamperometry experiments), or swept up and down at a certain scan rate (in voltammetry experiments). Any change in electrode potential also results in a capacitive current, whose contribution to the total current can be removed by subtracting a signal recorded under the same conditions but with no enzyme. As an example, SI figure S1B shows a catalytic voltammogram and a control signal, the difference between the two is the catalytic current. We only plot the latter (after subtraction of a blank) in the figures of the main text. Desorption of the enzyme film over time may result in a decrease in current, which in the favorable situations is slow enough that the effect is small or can be corrected[33]. The three enzymes discussed in this paper formed very stable films.

Figure 2 compares the voltammetric signatures of Cr, CpIII and MeII FeFe hydrogenases adsorbed onto a rotating pyrolytic graphite edge electrode in a solution saturated with H_2. The CpIII signal in figure 2 (red) is the same as that published in ref [5] (except the potential window is different), very similar to that of MeII (orange), and very distinct from that of Cr HydA1 (green) and other prototypical hydrogenases[34]. The CpIII and MeII enzymes completely inactivate on the scan towards high potentials, above E = -100 mV, but this inactivation is reversible: on the scan towards low potential, a large fraction of the activity is recovered under very reducing conditions (below -400mV): compare in figure 2 (red trace) the approx. 90% decrease from forward to backward scan at -0.2 V vs the 25% decrease between the beginning and the end of the cycle, when the potential is back to at -0.5 V. The slight loss of current when the low potential limit of the cyclic voltammogram (CV) is reached can be due to incomplete reactivation on this particular time scale or film loss[33]. SI figure S1A shows in red the subsequent scan, which demonstrates that the H_2-oxidation activity is also mostly recovered by the excursion to low potentials, and in blue another subsequent scan recorded after a poise to low potential: the reactivation is then complete. This implies that the surface coverage is nearly constant on the time scale of one or two CVs (about 100 s), and that the large variations in current that we observe during each potential sweep are due to changes in activity, rather than film loss or any other process that would lead to irreversible current decay (as sometimes occurs, see e.g. ref [35–37]).

The CpIII, MeII and Cr HydA1 CVs shown as plain lines in figure 2 were recorded with the enzyme in a chloride-free buffer at 30°C. Addition of chloride has little effect on the shape and magnitudes of the CpIII and MeII CVs (SI figure S2). The reversible oxidative inactivation occurs at a lower potential and is distinct from that of Cr HydA1 and other group A FeFe hydrogenases : the latter is strictly dependent on the presence of chloride (or bromide) in the buffer[34], as shown by the dashed line in figure 2. The shape of the CpIII and MeII CVs is reminiscent of that of Cb (gray line in figure 2)[14], although the mechanism appears to be distinct hereafter.

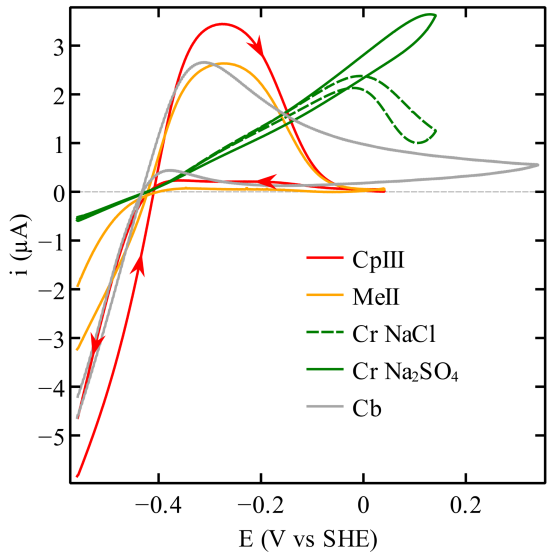

Figure 2: Cyclic voltammetry of CpIII (red), MeII (orange), Cb (gray) and Cr HydA1 (green), all at pH 7 under one atm. of H_2. The signals shown in solid lines were recorded without chloride, those shown in a dashed line in the presence of 0.1M chloride. The Cb voltammogram was scaled down three-fold to ease the comparison. The Cr HydA1 voltammogram with NaCl was scaled up 1.3 times to compensate for film-loss and allow a proper comparison with the voltammogram with Na_2SO_4. Arrows show the directions of the sweeps. A capacitive current recorded in an experiment without enzyme was subtracted from each voltammogram. Conditions: 30°C (except Cb, 5°C); scan rate : 20 mV/s; electrode rotation rate : 3000 rpm.

Figures 3A and B show a series of CpIII CVs recorded at 5°C (A) and 30°C (B) with the same film and increasing values of the high potential limit (where the sweep is reversed) from red to blue. The enzyme was reactivated by a reductive poise at -509 mV for two to three minutes between each CV (the resulting reactivation is demonstrated in the above discussion of figure 2 and S1A). Note that the exact value of the low potential that we used to trigger reactivation does not matter. It results from a compromise: the rate of reactivation increases at low potential (see below the discussion of figure 4D), but we observed that CpIII, like other FeFe hydrogenases[38,39], also inactivates when the conditions are too reducing (for a reason that is still not clear). Here a very slow decay in current over time is observed (about -30% in 1000 seconds), resulting from film loss or other irreversible processes, and responsible for the change in the maximal current between the 1st and the last CV in fig 3B. This was taken into account in the quantitative analysis of the voltammograms described below, as a variable value of the limiting current for each CV.

The CVs at 5°C in panel A clearly show that the reactivation consists of two different processes. One occurs around -150 mV and results in a sigmoidal increase in current at about the same potential as the inactivation seen on the upward sweep. But this reactivation is not complete (in the CVs recorded with the most positive vertex potential, the current at -0.2 V during the reductive sweep is about 25% of the current of the oxidative sweep): full activity is only recovered at much lower potential, during the reductive poise.

This shows that two distinct inactive species, distinguished by their reactivation kinetics, are produced under oxidizing conditions. In the following we call I_1 and I_2 the species that reactivate at high and low potential, respectively.

The sigmoidal variations of activity seen around -150 mV, and the observation that the potentials where I_1 is formed (on the sweep upward) and reactivates (on the sweep backward) are very similar, suggest that I_1 is in equilibrium with the active form of the enzyme on the time scale of the voltammetry. That this (in)activation is still clearly observed in voltammograms recorded at a much faster scan rate (up to 0.5 V/s in SI figure S5) confirms that it results from a fast reaction. That full reactivation of the enzyme at low potential required a reductive poise (figures 3A and B) shows that the reactivation of the other inactive state, I_2, is much slower than that of I_1.

That the sigmoidal reactivation around -150 mV is clearly visible only at 5°C, and not at 30°C, suggests that at high temperature, the formation of I_2 becomes fast enough that the entire sample is converted into I_2, a species that reactivates only under very reducing conditions.

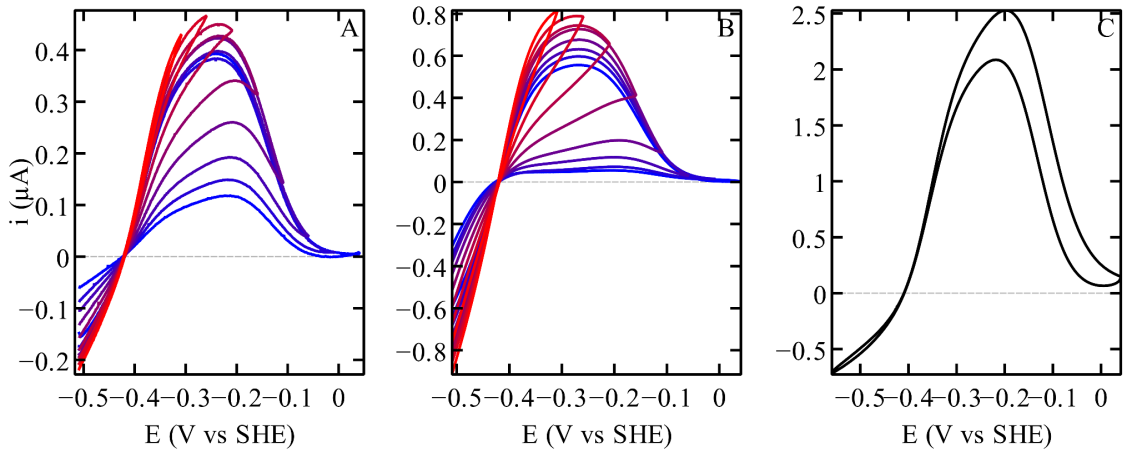

Figure 3: Cyclic voltammograms of WT CpIII recorded by changing the upper potential limits (red to blue from the lower to the greater vertex potential) at 5°C (panel A) and 30°C (panel B). Cyclic voltammogram of the CpIII mutant, missing the supernumerary cysteine of the TSCCCP motif, at 30°C (panel C). The capacitive current recorded in experiments carried out without enzyme was subtracted from all the voltammograms. Other conditions: pH 7; 20 mV/s; 3000 rpm.

The variable high-potential limit experiments in figures 3A and B suggest that I_1 is not an intermediate between the active form of the enzyme and I_2. Indeed, if this were to be the case (hypothesis 1 in scheme 1), any increase in the vertex potential (below -150 mV) would cause an exponential increase in the rate of formation of I_2. Instead, the data suggest that the slightly larger amount of I_2 produced when the vertex potential is increased is the mere consequence of the time spent at high potential being greater. Similarly, it seems possible to rule out the hypothesis that I_2 is produced from the active form of the enzyme only (hypothesis 2 in scheme 1): in that case,

increasing the high potential limit of the sweep would prevent the formation of I_2, since under these conditions I_1 would accumulate more. The qualitative inspection of the CVs therefore suggests that I_2 is produced upon oxidation of either A or I_1 (hypothesis 3 in scheme 1). This hypothesis is supported by the quantitative analysis of the voltammetry below.

We quantitatively analyze the data recorded at 30°C (rather than 5°C), because we are interested in the kinetics of formation and reactivation of I_2, which is more easily obtained at 30°C, the reactivation of I_2 being too slow at 5°C.

We used the following assumptions to fit a model to the CVs in figure 3B.

- The active enzyme molecules transform into two fully inactive species, I_1 and I_2.

$$\Gamma = [\mathrm{A}] + [\mathrm{I_1}] + [\mathrm{I_2}] \quad (1)$$

  where Γ is the constant, total enzyme surface coverage, and the square brackets indicate surface concentrations (all in units of mol/cm^2).

- The observed catalytic current $i(E,t)$ is the product of the steady-state response of the active enzyme times the time-dependent fraction of active enzyme [40,41]:

$$i(E,t) = i_{\mathrm{stat}}(E) \times [\mathrm{A}](t) \quad (2)$$

- The steady-state catalytic response of the active enzyme is modeled by the generic "EECr" equation[41,42].
- I_1 is in redox equilibrium with the active enzyme.

$$\frac{[\mathrm{I_1}]}{[\mathrm{A}]} = \exp\left(\frac{F}{RT}(E - E_1^0)\right) \quad (3)$$

  (we expect $E°_1$ around -150 mV).

- I_2 is produced slowly (on the time scale of the voltammetry) either from I_1 (hypothesis 1), from A (hypothesis 2), or indistinctly from either A or I_1 (hypothesis 3), as depicted in scheme 1. If we note k_i the pseudo 1st-order rate constant of production of I_2 (inactivation) and k_a the rate of disappearance of I_2 (activation), the hypotheses translate into:

$$\text{hypothesis 1: } d[\mathrm{I_2}]/dt = k_i[\mathrm{I_1}] - k_a[\mathrm{I_2}] \quad (4)$$

$$\text{hypothesis 2: } d[\mathrm{I_2}]/dt = k_i[\mathrm{A}] - k_a[\mathrm{I_2}] \quad (5)$$

$$\text{hypothesis 3: } d[\mathrm{I_2}]/dt = k_i([\mathrm{A}] + [\mathrm{I_1}]) - k_a[\mathrm{I_2}] \quad (6)$$

- The rate constants k_i and k_a depend on potential in a sigmoidal manner:

$$k_i = \frac{k_i^{\max}}{1 + \exp\left(\frac{-F}{RT}(E - E_2^0)\right)} \quad (7)$$

$$k_a = \frac{k_a^{\max}}{1 + \exp\left(\frac{F}{RT}(E - E_3^0)\right)} \quad (8)$$

  Note that k_i tends to k_i^{max} at high potential, and k_a tends to k_a^{max} at low potential. This (in)activation kinetics is expected if the formation of I_2 follows an "ECE" mechanism (using the electrochemical terminology), with an oxidation (e.g. the formation of H_{ox}, the most oxidized catalytic intermediate) that precedes the inactivation, a chemical transformation,

and a final oxidation that locks the inactive state. But we make no a priori assumption on the values of E^0_2 and E^0_3.

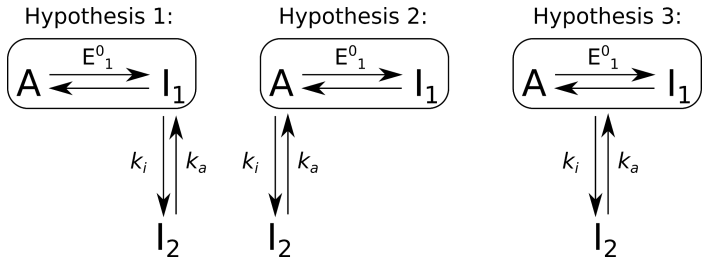

Scheme 1. The three tested hypotheses regarding the inactivation kinetics, according to which the 2nd inactive species (I_2) is produced either from the 1st one (hypothesis 1), from the active form (A) (hypothesis 2), or from both at the same rate. The rectangles group species that are supposed to remain at equilibrium with one another. The dependence of k_i and k_a on E is given by eqs 7 and 8 (which include E^0_2 and E^0_3 as parameters).

We used the QSoas software[43] to fit the model to two successive scans to accurately determine the kinetics of slow reactivation at low potential. Figure 4 shows the best fit of the 3rd model to three selected voltammograms of WT CpIII at pH 7, 30°C (the model was fitted to all the CVs shown in figure 3B globally, we show only 3 CVs in figure 4 for clarity). The other two hypotheses gave less satisfactory modeling (SI figures S3 and S4), as expected from the above qualitative discussion of figure 3. That the 3rd hypothesis gives the best fit of the voltammetry implies that the two inactivation processes are independent of one another. It may be, for example, that one corresponds to a transformation of the active site, and the other results from a remote process.

Figure 4D shows the dependence of k_i and k_a on E that is deduced from the global fitting procedure. We obtained k_i^{max}=0.08 s^{-1}, k_a^{max}=0.08 s^{-1}, E^0_1=-139 mV, E^0_2=-317 mV, and E^0_3=-384 mV for CpIII at 30°C, pH 7. We estimated that the errors on E^0_2 and E^0_3 (the parameters defined in eqs 7 and 8) are around ± 50 mV. The value of E^0_1 defines the equilibrium between the active enzyme and I_1 at high potential. The value of E^0_2 is that of the redox step that precedes the oxidative formation of I_1; here it is close to the potential of H_{red}/H_{ox} measured in IR titrations of prototypical hydrogenases (this parameter has not been measured for CpIII), and the value of E^0_3 is close to the value of the reduction potential of the H_{ox}/H_{ox+1} transition in CpIII (-380 mV at pH 8 in ref [5]), suggesting that the I_2 inactive species is H_{ox+1}, i.e. H_{inact} (according to our hypothesis in the discussion of this paper).

The pH dependence of the parameters obtained by analyzing voltammetric data recorded in the range of pH 7-9.5 is shown in SI figure S6. It supports the above hypothesis that the I_2 inactive species corresponds to H_{inact}. Indeed, the parameter k_i^{max} is pH independent (like the rate constant of formation of H_{inact} in *C. beijerinckii* hydrogenase[14]); moreover, the potential E^0_3, which presumably corresponds to the reduction of H_{inact}, decreases 60 mV/pH, and k_a^{max} is pH independent. This results in an increase of the reactivation rate when the pH is decreased, consistent with the observations regarding the reactivation kinetics of H_{inact} in Cb[14] and in prototypical hydrogenases[22]. The value of E^0_1 also depends on pH.

In an effort to identify the functional significance of the supernumerary cysteine in the TSCCCP motif, we produced the ΔC223 CpIII variant, by deleting one of the three adjacent cysteine residues. The deletion does not change the catalytic bias, as shown by the CV of the ΔC223 variant in figure 3C, but

significantly decreases the overall activity (see the assays section in SI). However, the shape of the CV is very different from that of WT CpIII and MeII. In particular, the inactivation seems to involve only the I_1 species (which is produced and reactivated at high potential). Indeed, the reactivation at high potential is more pronounced than with the WT and complete. A small hysteresis is observed at high potential; it may also be present in the WT voltammetry but hidden by the second inactivation process (the formation of I_2), which is not detected in the variant. The potential of the fast inactivation in the ΔC223 variant, simply obtained from the position of the inflection in the voltammetry, is the same as in the wild type enzyme, over a range of pH values (SI figure S6A).

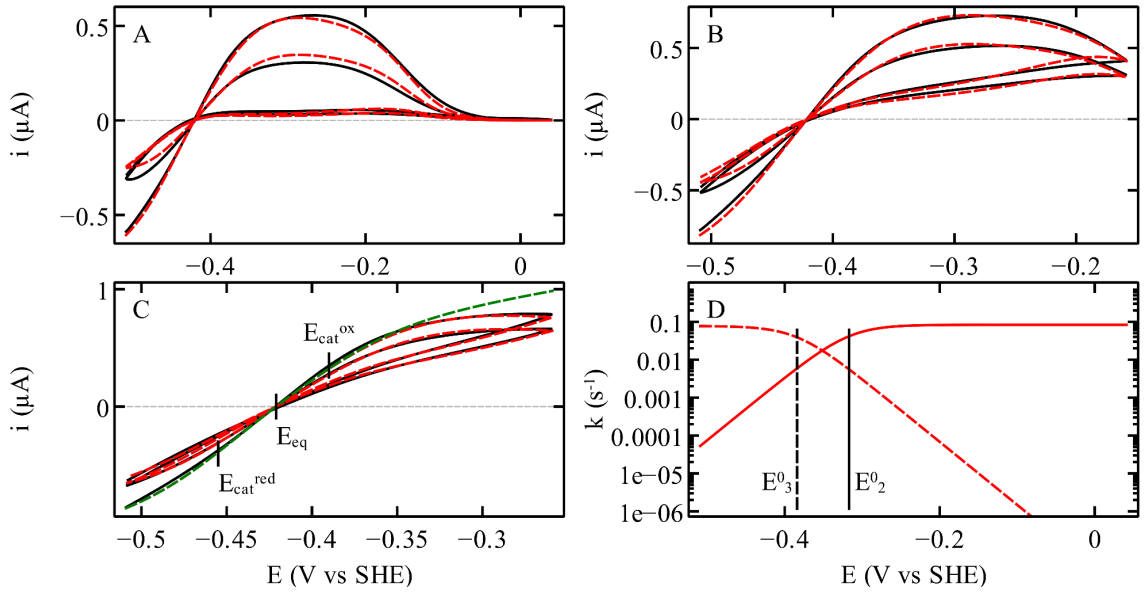

Figure 4: fit of the 3rd model to three selected voltammograms of WT CpIII among those of figure 3B. Panels A, B and C show the experimental data in black and the fits of the 3rd model in dash red lines. Panel D shows the potential dependence of k_i (solid line) and k_a (dash line) obtained from the global fit[43]. The green dashed line in panel C shows the steady state catalytic response simulated from the parameters of the best fit, by forcing the inactivation rate constants to be zero. Vertical lines in panel C indicate the two catalytic potentials E_{cat}^{ox} and E_{cat}^{red} and the equilibrium potential E_{eq}. Solid and dashed vertical lines in panel D note the values of E^0_2 and E^0_3, respectively.

In addition to the (in)activation kinetics, the outcome of the fitting procedure is the steady-state response of the fully active enzyme (green in figure 4C) [41,42]. The latter is defined by two catalytic potentials, E_{cat}^{ox} and E_{cat}^{red}. The difference between (E_{cat}^{ox} + E_{cat}^{red})/2 and E_{eq}, the H^+/H_2 Nernst potential, gives the catalytic bias of the enzyme, defined as the ratio of the oxidative and reductive limiting currents, which would be observed in the absence of any inactivation process.

$$\frac{i_{\mathrm{lim}}^{\mathrm{ox}}}{i_{\mathrm{lim}}^{\mathrm{red}}} = \exp\left[\frac{2F}{RT}\left(\frac{E_{\mathrm{cat}}^{\mathrm{ox}} + E_{\mathrm{cat}}^{\mathrm{red}}}{2} - E_{\mathrm{eq}}\right)\right] \quad (9)$$

Table 2 shows the values of the catalytic bias of CpIII and Cr HydA1, at pH 7, based on the analysis of the voltammograms shown in figures 2 and 4. SI figure S6F shows the value of the two catalytic potentials in the pH range from 7 to 9.5 for CpIII WT. We conclude that the intrinsic catalytic bias is about the same in all cases, with the enzymes being equally active in both directions of the reaction. Only a small increase in bias in the direction of H_2 oxidation is detected above pH 8.5.

Table 2. The catalytic potentials (in mV vs SHE) and catalytic bias under one atm. of H_2 of Cr HydA1 and CpIII at 30°C, pH 7, 1 bar H_2, E_{eq} = -419 ± 2 mV.

	E_{cat}^{ox}	E_{cat}^{red}	$(E_{cat}^{ox}+E_{cat}^{red})/2$	$i_{lim}^{ox}/i_{lim}^{red}$	figure
CpIII	-390	-455	-423	0.85	4
Cr	-362	-448	-405	2.5	2

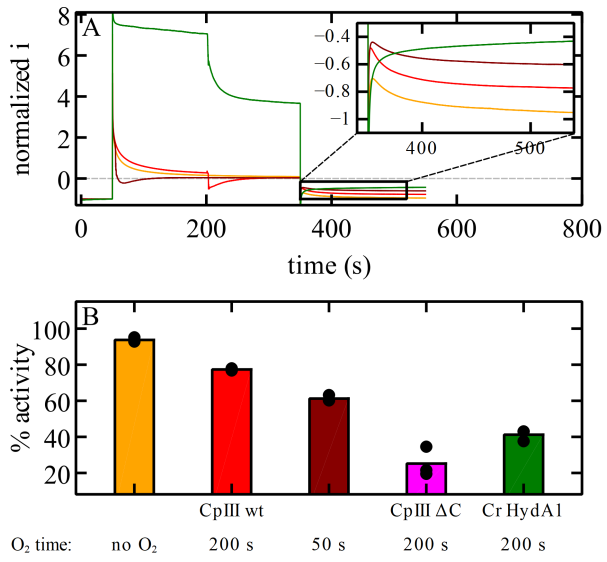

Figure 5: Panel A: chronoamperometric experiments to compare the reaction with O_2 of the enzymes Cr HydA1 (green) and CpIII (shades of red), and to evidence the protection from O_2 that is afforded by the formation of the inactive state I_2. The electrode potential was stepped from -459 mV to -249 mV (avoiding higher potentials to not produce I_1) and then back to -459 mV. The current is normalized by its value during the initial reductive poise, so that the current values observed during the second reductive poise can be easily compared. In some experiments 70 µM of O_2 was added to the cell solution, either immediately (dark red) or after 150 s of oxidative poise (red and green), to inactivate the enzyme. The orange line is an anaerobic control performed with CpIII, in which the enzyme experienced the oxidative poise without any O_2 exposure. Conditions: 30°C; pH 7; 3000 rpm. Panel B: summary of the values obtained in these experiments (average of three different experiments, each shown as a dot). The color code is the same as in panel A.

Our attempts to produce the enzyme CpIII under aerobic conditions led to an inactive enzyme. Exposing the sample of anaerobically produced enzyme to air also inactivated it. We tested the effect of short exposures to O_2 in chronoamperometry experiments. Figure 5 compares chronoamperograms recorded with Cr HydA1 (a prototypical, O_2-sensitive FeFe hydrogenase[44]) and CpIII. The electrode was first poised at a low potential (-459 mV), to measure a reference

H_2-evolution current. The potential was then stepped to -249 mV to drive H_2 oxidation and the formation of only the I_2 inactive species, and 70 µM of O_2 was added to the cell solution, either immediately after the step up (at 50 s) or after 150 s of oxidative poise (at 200 s), to inactivate the enzyme. Anaerobicity was then restored in about 100 s by the continuous flush of H_2 (in these experiments, the O_2 concentration decayed exponentially[45] with a time constant of 30 s). A final poise to the initial potential was used to measure the reductive catalytic current that could be compared to the initial value to estimate the damage resulting from transient exposure to O_2.

The Cr HydA1 signal (green) shows no anaerobic inactivation (because there is no chloride in the buffer, the small decrease in current results from film loss); addition of O_2 decreases the activity by a factor of two, and after stepping the potential down, the observed reductive current is also half as small as its initial value. The orange line is an anaerobic control performed with CpIII, showing that oxidative inactivation is fully reversible (the final and initial current values are nearly identical, which also suggests that film loss is minimal). The dark red and red experiments performed with CpIII show that the earlier the addition of O_2 after the step to high potential, the smaller the final activity when reducing conditions are restored, showing that anaerobic oxidative inactivation protects the enzyme from O_2. The result shown in purple was obtained with the ΔC223 variant (in this variant, the I_2 state is not formed, cf the above discussion of fig 3C). The current recovered after the exposure to O_2 is much lower than that obtained with the WT enzyme under the same conditions (dark red). This shows that the supernumerary cysteine is required for the formation of the O_2-protected state I_2.

Discussion

There has been much interest recently in the reaction of the H-cluster of prototypical[21,22,46] and atypical hydrogenases[14,47] from group A (Cr HydA1 and Cb, respectively) with extrinsic or intrinsic sulfide. The formation of the sulfide-bound oxidized inactive state is revealed by a particular FTIR signature called H_{inact} and reversed upon reduction. CpIII is another example of hydrogenase that can be oxidized to a state, called H_{ox+1} in ref [5], that is very similar to the H_{inact} state, whereas it belongs to the phylogenetically distinct group B. The relations between the formation of H_{ox+1} in CpIII, inactivation and protection from O_2 have not been discussed. The structural determinants of this reaction in CpIII were also unknown, but we have been intrigued by the cysteine-rich TSCCCP motif present in CpIII and other group B FeFe hydrogenases, such as MeII. This motif defines the subgroup "B2"[12].

In the absence of a crystallographic structure of any FeFe hydrogenase from group B, we examined an AlphaFold prediction of the structure of CpIII hydrogenase (figures 1, S8, S9). The overall fold was already predicted to be very similar to that of standard hydrogenases (SI figure S6 in ref [5]). The AlphaFold model shown here in figure 1A suggests that the sulfur of the supernumerary cysteine (C221) is involved in proton transfer.

Redox-driven inactivation is a usual feature of FeFe hydrogenases, but significant variations have recently been observed. Oxidative, reversible inactivation is observed with CpI and other prototypical FeFe hydrogenases from group A, but it occurs only under very oxidizing conditions and only in the presence of chloride, bromide[34] or sulfide[22]. All experiments herein were performed in a chloride- and sulfide-free buffer, which implies that the mechanism of inactivation is distinct.

Reversible oxidative inactivation occurs with *Clostridium beijerinckii* FeFe hydrogenase (Cb, also from group A, gray in figure 2) in the absence of chloride or exogenous sulfide, and it results from the

formation of the H_{inact} state upon binding to the distal Fe of the H-cluster of the sulfur of the cysteine that is equivalent to CpI C299[14,47,48] (see figure 1A). From the observation that CpIII is also oxidized to a state whose signature is very similar to that of the H_{inact} state in the absence of sulfide (Table S3 in ref [5]), we hypothesize that the binding of the cysteine to Fe_d occurs in CpIII, as it does in Cb. This is probably one of the two reasons CpIII inactivates at high potential. The slow reduction of this H_{inact}-like state may be the cause of the lag observed in solution assays of CpIII (SI section 1.2 in ref [5]). The voltammetry of CpIII and MeII being very similar, it is tempting to suggest that this bond formation also occurs in MeII and other hydrogenases from group B. The oxidative formation of a vicinal disulfide bridge[49] between C222 and C221 may also result in enzyme inactivation, but this alternative hypothesis does not explain the observation of the H_{inact} state, so we considered it unlikely.

The voltammetric signatures of CpIII and MeII in figure 2 may look similar to that of Cb at first (figure 2). However we observed that the (in)activation kinetics of CpIII and MeII is different from that of Cb. In particular two distinct inactive species, referred to here as I_1 and I_2, are produced independently.

We consider most likely that the 2nd inactive species (I_2) is the H_{inact} state. Indeed, the reduction of H_{inact} occurs at low potential (-400 mV at pH 8 according to the results in ref [5]), which matches the reactivation kinetics of I_2 (E^0_3 = -384 mV at pH 7, according to the above described modeling of the voltammetry). The pH dependence of the (in)activation kinetics in CpIII also supports this hypothesis (cf the above discussion of SI figure S6).

The observation that the binding of the cysteine and the formation of H_{inact} occur in these group B enzymes, which are phylogenetically distinct from Cb, is intriguing. The three residues that have been identified as allowing the formation of H_{inact} in Cb by making the TSCCP loop flexible (L364, P386 and A561)[50] are not conserved in CpIII and MeII (see the orange frames in SI figure S7), but we observed that in CpIII, this inactivation disappears when the supernumerary cysteine is deleted. This suggests that in WT CpIII, C221 pushes the proximal cysteine (C222) closer to Fe_d and hence favors the formation of the Fe_d-Scys222 bond. It therefore appears that different peculiar structural features in Cb on one side, and group B2 hydrogenases on the other, give the protein the ability to allow the proximal cysteine to bind Fe_d.

Binding of a nearby residue to Fe_d should protect the H-cluster from O_2. This is so in Cb, but the same protection mechanism operates in a certain type of NiFe hydrogenases, where the binding to a metal ion of the active site of a nearby aspartate protects the enzyme from oxygen attack[51,52]. However, we have found no evidence that CpIII hydrogenase can be exposed to air for long periods without losing activity, despite the fact that the I_2/H_{inact} oxidized inactive state of WT CpIII, like H_{inact} of Cb[14], is protected from O_2 (figure 5). This is probably because the formation of H_{inact} is too slow (0.08 s^{-1} at 30°C in CpIII, compared to 1 s^{-1} at 5°C in Cb [14]), so that the disruption of the active site by O_2 occurs faster than the enzyme can protect itself by forming the H_{inact} state. The relation between fast formation of H_{inact} and greater resistance was demonstrated before in a series of Cb site directed mutants [14,15].

The other inactive species, I_1, is produced and reduced more quickly and at much higher potential (-150 mV) than I_2, irrespective of the presence of the third cysteine in the P1 motif (that is, in WT CpIII and in the ΔC variant, figure 3C). Since the formation of I_2 occurs independently from the production of I_1 at the active site (hypothesis 3 in the modeling of the voltammetry), this inactivation,

which is not affected by the change in coordination of Fe_d, and not affected either by the deletion of the supernumerary cysteine (figure 3C and SI figure S6), must be the consequence of a remote transformation. The molecular mechanism of this fast oxidative inactivation is not clear at that stage. We may consider that it results from the overoxidation of an accessory cluster, maybe the distal cluster whose coordination pattern is very peculiar in group B hydrogenases (SI figure S9), but this redox process was not detected in the EPR titration reported in ref [5] (SI figure S7 therein, where the enzyme is oxidized up to -28 mV at pH 8).

To discuss the catalytic bias and the shape of the voltammograms, one needs to acknowledge that the catalytic response of the enzyme is modulated by the inactivation processes: the observed voltammogram is actually the product of the steady-state response of the active enzyme (an intrinsic property of the active site) times the time-dependent fraction of enzyme that is active (considering the two redox-dependent, reversible inactivation processes, eq 2). The quantitative modeling of the voltammetry (figure 4) allows us to untangle the two contributions, to obtain the steady-state response (green in figure 4C) and the kinetics of inactivation. The shape of the former tells whether the enzyme is an equally good catalyst in the two directions of the reaction, or if it is biased in one particular direction. This is quantified by the difference between the average catalytic potential and the Nernst potential of the H^+/H_2 couple (eq 9)[42]. Table 2 shows that CpIII hydrogenase is actually not intrinsically biased in any direction (the ratio of the limiting currents is close to one), just like Cr HydA1. This contrasts with the observation that in solution assays, CpIII is much more active in the reductive than in the oxidative direction[5]. The reason for this apparent discrepancy is that in solution assays, the enzyme inactivates under the oxidative conditions that are required to drive H_2 oxidation, hence the very small oxidative activity. The same is true for Cb, which is very efficient at oxidizing H_2, but whose strong H_2-oxidation activity is hidden by the oxidative inactivation, except in some variants where this inactivation is slowed (fig 3d in ref [14]).

If one is interested in using the enzyme to catalyze H_2 oxidation, that it inactivates under oxidative condition is clearly an issue that has to be considered. However, if one's goal is to elucidate how the residues that surround the H-cluster may tune its catalytic properties and the catalytic bias, then any redox driven inactivation must be factored out. Here, we conclude that the properties of the active site of CpIII hydrogenase are not very different from those of group A hydrogenases (e.g. Cb or Cr HydA1), in that the enzyme is intrinsically equally active in both directions. That Cb and CpIII hydrogenase inactivate at high potential does not reveal any difference in terms of H-cluster redox and catalytic properties.

Further spectroscopic investigations will be needed to unequivocally identify and characterize the two inactive states. This will require producing larger amounts of enzyme than we have been able to. Of concern is also the lower specific activity of our WT CpIII samples with respect to previously published values[5]. This may merely result from differences in assay conditions, or reveal an inhomogeneity in our samples. The latter would decrease the apparent activity of the sample, but may not affect the protein film voltammetry results, on condition that each enzyme molecule is either fully active or fully inactive (as would occur if some enzyme molecules did not incorporate the active site): in that case, only the fully mature proteins contribute to the PFV signal. The quantitative analysis of the voltammetry does not suggest otherwise.

Supporting Information

The electrochemical data are available on the Zonodo repository at doi: 10.5281/zenodo.10948191. Molecular biology and biochemistry procedures, additional electrochemical experiments and data analyses, sequence alignments, structural considerations, available free of charge at doi: 10.1021/acscatal.4c01352 .

Acknowledgements

We thank Miriam Malagnini for performing some of the experiments included in the revision of this paper, and Martin Winkler and Jan Jaenecke for assistance and helpful discussions. This research was funded by the Centre National de la Recherche Scientifique, Aix Marseille Université, Agence Nationale de la Recherche (ANR-21-21-CE50-0041), Région Sud. This work received support from the french government under the France 2030 investment plan, as part of the Initiative d'Excellence d'Aix-Marseille Université – A*MIDEX, AMX-22-RE-AB-097. The authors are very grateful to Frédérique Berger, glass blower at Aix Marseille University and the proteomic facility of the Institut de Microbiologie de la Méditerranée (IMM, CNRS-AMU, FR3479), Marseille Proteomique (MaP), for performing proteomic analyses by mass spectrometry.

References

(1) Sommer, C.; Adamska-Venkatesh, A.; Pawlak, K.; Birrell, J. A.; Rüdiger, O.; Reijerse, E. J.; Lubitz, W. Proton Coupled Electronic Rearrangement within the H-Cluster as an Essential Step in the Catalytic Cycle of [FeFe] Hydrogenases. *J. Am. Chem. Soc.* **2017**, *139* (4), 1440–1443. https://doi.org/10.1021/jacs.6b12636 .

(2) Laun, K.; Baranova, I.; Duan, J.; Kertess, L.; Wittkamp, F.; Apfel, U.-P.; Happe, T.; Senger, M.; Stripp, S. T. Site-Selective Protonation of the One-Electron Reduced Cofactor in [FeFe]-Hydrogenase. *Dalton Trans.* **2021**, *50* (10), 3641–3650. https://doi.org/10.1039/d1dt00110h .

(3) Duan, J.; Senger, M.; Esselborn, J.; Engelbrecht, V.; Wittkamp, F.; Apfel, U.-P.; Hofmann, E.; Stripp, S. T.; Happe, T.; Winkler, M. Crystallographic and Spectroscopic Assignment of the Proton Transfer Pathway in [FeFe]-Hydrogenases. *Nat. Commun.* **2018**, *9* (1), 4726. https://doi.org/10.1038/s41467-018-07140-x .

(4) Morra, S.; Arizzi, M.; Valetti, F.; Gilardi, G. Oxygen Stability in the New [FeFe]-Hydrogenase from Clostridium Beijerinckii SM10 (CbA5H). *Biochemistry* **2016**, *55* (42), 5897–5900. https://doi.org/10.1021/acs.biochem.6b00780 .

(5) Artz, J. H.; Zadvornyy, O. A.; Mulder, D. W.; Keable, S. M.; Cohen, A. E.; Ratzloff, M. W.; Williams, S. G.; Ginovska, B.; Kumar, N.; Song, J.; McPhillips, S. E.; Davidson, C. M.; Lyubimov, A. Y.; Pence, N.; Schut, G. J.; Jones, A. K.; Soltis, S. M.; Adams, M. W. W.; Raugei, S.; King, P. W.; Peters, J. W. Tuning Catalytic Bias of Hydrogen Gas Producing Hydrogenases. *J. Am. Chem. Soc.* **2020**, *142* (3), 1227–1235. https://doi.org/10.1021/jacs.9b08756 .

(6) Peters, J. W.; Lanzilotta, W. N.; Lemon, B. J.; Seefeldt, L. C. X-Ray Crystal Structure of the Fe-Only Hydrogenase (CpI) from Clostridium Pasteurianum to 1.8 Angstrom Resolution. *Science* **1998**, *282* (5395), 1853–1858. https://doi.org/10.1126/science.282.5395.1853 .

(7) Morra, S. Fantastic [FeFe]-Hydrogenases and Where to Find Them. *Front. Microbiol.* **2022**, *13*, 853626. https://doi.org/10.3389/fmicb.2022.853626 .

(8) Bairoch, A.; Bucher, P. PROSITE: Recent Developments. *Nucleic Acids Res.* **1994**, *22* (17), 3583–3589.

(9) Vignais, P. M.; Billoud, B. Occurrence, Classification, and Biological Function of Hydrogenases: An

Overview. *Chem. Rev.* **2007**, *107* (10), 4206–4272. https://doi.org/10.1021/cr050196r .
(10) Greening, C.; Biswas, A.; Carere, C. R.; Jackson, C. J.; Taylor, M. C.; Stott, M. B.; Cook, G. M.; Morales, S. E. Genomic and Metagenomic Surveys of Hydrogenase Distribution Indicate H2 Is a Widely Utilised Energy Source for Microbial Growth and Survival. *ISME J.* **2016**, *10* (3), 761–777. https://doi.org/10.1038/ismej.2015.153 .
(11) Calusinska, M.; Happe, T.; Joris, B.; Wilmotte, A. The Surprising Diversity of Clostridial Hydrogenases: A Comparative Genomic Perspective. *Microbiology* **2010**, *156* (Pt 6), 1575–1588. https://doi.org/10.1099/mic.0.032771-0 .
(12) Meyer, J. [FeFe] Hydrogenases and Their Evolution: A Genomic Perspective. *Cell. Mol. Life Sci.* **2007**, *64* (9), 1063–1084. https://doi.org/10.1007/s00018-007-6477-4 .
(13) Fasano, A.; Fourmond, V.; Léger, C. Outer-Sphere Effects on the O2 Sensitivity, Catalytic Bias and Catalytic Reversibility of Hydrogenases. *Chem. Sci.* **2024**, *15* (15), 5418–5433. https://doi.org/10.1039/D4SC00691G .
(14) Winkler, M.; Duan, J.; Rutz, A.; Felbek, C.; Scholtysek, L.; Lampret, O.; Jaenecke, J.; Apfel, U.-P.; Gilardi, G.; Valetti, F.; Fourmond, V.; Hofmann, E.; Léger, C.; Happe, T. A Safety Cap Protects Hydrogenase from Oxygen Attack. *Nat. Commun.* **2021**, *12* (1), 756. https://doi.org/10.1038/s41467-020-20861-2 .
(15) Rutz, A.; Das, C. K.; Fasano, A.; Jaenecke, J.; Yadav, S.; Apfel, U.-P.; Engelbrecht, V.; Fourmond, V.; Léger, C.; Schäfer, L. V.; Happe, T. Increasing the O2 Resistance of the [FeFe]-Hydrogenase CbA5H through Enhanced Protein Flexibility. *ACS Catal.* **2023**, *13* (2), 856–865. https://doi.org/10.1021/acscatal.2c04031 .
(16) Cabotaje, P. R.; Walter, K.; Zamader, A.; Huang, P.; Ho, F.; Land, H.; Senger, M.; Berggren, G. Probing Substrate Transport Effects on Enzymatic Hydrogen Catalysis: An Alternative Proton Transfer Pathway in Putatively Sensory [FeFe] Hydrogenase. *ACS Catal.* **2023**, *13* (15), 10435–10446. https://doi.org/10.1021/acscatal.3c02314 .
(17) Land, H.; Sekretareva, A.; Huang, P.; Redman, H. J.; Németh, B.; Polidori, N.; Mészáros, L. S.; Senger, M.; Stripp, S. T.; Berggren, G. Characterization of a Putative Sensory [FeFe]-Hydrogenase Provides New Insight into the Role of the Active Site Architecture. *Chem. Sci.* **2020**, *11* (47), 12789–12801. https://doi.org/10.1039/d0sc03319g .
(18) Fasano, A.; Land, H.; Fourmond, V.; Berggren, G.; Léger, C. Reversible or Irreversible Catalysis of H+/H2 Conversion by FeFe Hydrogenases. *J. Am. Chem. Soc.* **2021**, *143* (48), 20320–20325. https://doi.org/10.1021/jacs.1c09554 .
(19) Fasano, A.; Baffert, C.; Schumann, C.; Berggren, G.; Birrell, J. A.; Fourmond, V.; Léger, C. Kinetic Modeling of the Reversible or Irreversible Electrochemical Responses of FeFe-Hydrogenases. *J. Am. Chem. Soc.* **2024**. https://doi.org/10.1021/jacs.3c10693 .
(20) Fourmond, V.; Plumeré, N.; Léger, C. Reversible Catalysis. *Nature Reviews Chemistry* **2021**, *5* (5), 348–360. https://doi.org/10.1038/s41570-021-00268-3 .
(21) Rodríguez-Maciá, P.; Reijerse, E. J.; van Gastel, M.; DeBeer, S.; Lubitz, W.; Rüdiger, O.; Birrell, J. A. Sulfide Protects [FeFe] Hydrogenases From O2. *J. Am. Chem. Soc.* **2018**, *140* (30), 9346–9350. https://doi.org/10.1021/jacs.8b04339 .
(22) Felbek, C.; Arrigoni, F.; de Sancho, D.; Jacq-Bailly, A.; Best, R. B.; Fourmond, V.; Bertini, L.; Léger, C. Mechanism of Hydrogen Sulfide-Dependent Inhibition of FeFe Hydrogenase. *ACS Catal.* **2021**, *11* (24), 15162–15176. https://doi.org/10.1021/acscatal.1c04838 .
(23) Caserta, G.; Papini, C.; Adamska-Venkatesh, A.; Pecqueur, L.; Sommer, C.; Reijerse, E.; Lubitz, W.; Gauquelin, C.; Meynial-Salles, I.; Pramanik, D.; Artero, V.; Atta, M.; Del Barrio, M.; Faivre, B.; Fourmond, V.; Léger, C.; Fontecave, M. Engineering an [FeFe]-Hydrogenase: Do Accessory Clusters Influence O2 Resistance and Catalytic Bias? *J. Am. Chem. Soc.* **2018**, *140* (16), 5516–5526. https://doi.org/10.1021/jacs.8b01689 .
(24) Butt, J. N.; Filipiak, M.; Hagen, W. R. Direct Electrochemistry of Megasphaera Elsdenii Iron Hydrogenase. Definition of the Enzyme's Catalytic Operating Potential and Quantitation of the Catalytic Behaviour over a Continuous Potential Range. *Eur. J. Biochem.* **1997**, *245* (1), 116–122.

https://doi.org/10.1111/j.1432-1033.1997.00116.x .
(25) Hydrogenase Classifier - [FeFe] Group B http://web.archive.org/web/20230507103000/https://services.birc.au.dk/hyddb/browser/class/fefe-group-b/ (accessed Jun 9, 2023).
(26) Jumper, J.; Evans, R.; Pritzel, A.; Green, T.; Figurnov, M.; Ronneberger, O.; Tunyasuvunakool, K.; Bates, R.; Žídek, A.; Potapenko, A.; Bridgland, A.; Meyer, C.; Kohl, S. A. A.; Ballard, A. J.; Cowie, A.; Romera-Paredes, B.; Nikolov, S.; Jain, R.; Adler, J.; Back, T.; Petersen, S.; Reiman, D.; Clancy, E.; Zielinski, M.; Steinegger, M.; Pacholska, M.; Berghammer, T.; Bodenstein, S.; Silver, D.; Vinyals, O.; Senior, A. W.; Kavukcuoglu, K.; Kohli, P.; Hassabis, D. Highly Accurate Protein Structure Prediction with AlphaFold. *Nature* **2021**, *596* (7873), 583–589. https://doi.org/10.1038/s41586-021-03819-2 .
(27) Nicolet, Y.; Piras, C.; Legrand, P.; Hatchikian, C. E.; Fontecilla-Camps, J. C. Desulfovibrio Desulfuricans Iron Hydrogenase: The Structure Shows Unusual Coordination to an Active Site Fe Binuclear Center. *Structure* **1999**, *7* (1), 13–23. https://doi.org/10.1016/s0969-2126(99)80005-7 .
(28) Sievers, F.; Higgins, D. G. Clustal Omega for Making Accurate Alignments of Many Protein Sequences. *Protein Sci.* **2018**, *27* (1), 135–145. https://doi.org/10.1002/pro.3290 .
(29) Léger, C.; Bertrand, P. Direct Electrochemistry of Redox Enzymes as a Tool for Mechanistic Studies. *Chem. Rev.* **2008**, *108* (7), 2379–2438. https://doi.org/10.1021/cr0680742 .
(30) Sensi, M.; del Barrio, M.; Baffert, C.; Fourmond, V.; Léger, C. New Perspectives in Hydrogenase Direct Electrochemistry. *Current Opinion in Electrochemistry* **2017**, *5* (1), 135–145. https://doi.org/10.1016/j.coelec.2017.08.005 .
(31) del Barrio, M.; Guendon, C.; Kpebe, A.; Baffert, C.; Fourmond, V.; Brugna, M.; Léger, C. Valine-to-Cysteine Mutation Further Increases the Oxygen Tolerance of Escherichia Coli NiFe Hydrogenase Hyd-1. *ACS Catal.* **2019**, *9* (5), 4084–4088.
(32) Butt, J. N.; Jeuken, L. J. C.; Zhang, H.; Burton, J. A. J.; Sutton-Cook, A. L. Protein Film Electrochemistry. *Nature Reviews Methods Primers* **2023**, *3* (1), 1–19. https://doi.org/10.1038/s43586-023-00262-7 .
(33) Fourmond, V.; Lautier, T.; Baffert, C.; Leroux, F.; Liebgott, P.-P.; Dementin, S.; Rousset, M.; Arnoux, P.; Pignol, D.; Meynial-Salles, I.; Soucaille, P.; Bertrand, P.; Léger, C. Correcting for Electrocatalyst Desorption and Inactivation in Chronoamperometry Experiments. *Anal. Chem.* **2009**, *81* (8), 2962–2968. https://doi.org/10.1021/ac8025702 .
(34) Del Barrio, M.; Sensi, M.; Fradale, L.; Bruschi, M.; Greco, C.; de Gioia, L.; Bertini, L.; Fourmond, V.; Léger, C. Interaction of the H-Cluster of FeFe Hydrogenase with Halides. *J. Am. Chem. Soc.* **2018**, *140* (16), 5485–5492. https://doi.org/10.1021/jacs.8b01414 .
(35) Singh, K.; McArdle, T.; Sullivan, P. R.; Blanford, C. F. Sources of Activity Loss in the Fuel Cell Enzyme Bilirubin Oxidase. *Energy Environ. Sci.* **2013**, *6* (8), 2460–2464. https://doi.org/10.1039/C3EE00043E .
(36) Singh, K.; Blanford, C. F. Electrochemical Quartz Crystal Microbalance with Dissipation Monitoring: A Technique to Optimize Enzyme Use in Bioelectrocatalysis. *ChemCatChem* **2014**, *6* (4), 921–929. https://doi.org/10.1002/cctc.201300900 .
(37) Badiani, V. M.; Cobb, S. J.; Wagner, A.; Oliveira, A. R.; Zacarias, S.; Pereira, I. A. C.; Reisner, E. Elucidating Film Loss and the Role of Hydrogen Bonding of Adsorbed Redox Enzymes by Electrochemical Quartz Crystal Microbalance Analysis. *ACS Catal.* **2022**, *12* (3), 1886–1897. https://doi.org/10.1021/acscatal.1c04317 .
(38) Hajj, V.; Baffert, C.; Sybirna, K.; Meynial-Salles, I.; Soucaille, P.; Bottin, H.; Fourmond, V.; Léger, C. FeFe Hydrogenase Reductive Inactivation and Implication for Catalysis. *Energy Environ. Sci.* **2014**, *7* (2), 715–719. https://doi.org/10.1039/C3EE42075B .
(39) Megarity, C. F.; Esselborn, J.; Hexter, S. V.; Wittkamp, F.; Apfel, U.-P.; Happe, T.; Armstrong, F. A. Electrochemical Investigations of the Mechanism of Assembly of the Active-Site H-Cluster of [FeFe]-Hydrogenases. *J. Am. Chem. Soc.* **2016**, *138* (46), 15227–15233.

https://doi.org/10.1021/jacs.6b09366 .
(40) Barrio, M.; Fourmond, V. Redox (in)activations of Metalloenzymes: A Protein Film Voltammetry Approach. *ChemElectroChem* **2019**, *6* (19), 4949–4962. https://doi.org/10.1002/celc.201901028 .
(41) Fourmond, V.; Léger, C. Modelling the Voltammetry of Adsorbed Enzymes and Molecular Catalysts. *Current Opinion in Electrochemistry* **2017**, *1* (1), 110–120. https://doi.org/10.1016/j.coelec.2016.11.002 .
(42) Fourmond, V.; Wiedner, E. S.; Shaw, W. J.; Léger, C. Understanding and Design of Bidirectional and Reversible Catalysts of Multielectron, Multistep Reactions. *J. Am. Chem. Soc.* **2019**, *141* (28), 11269–11285. https://doi.org/10.1021/jacs.9b04854 .
(43) Fourmond, V. QSoas: A Versatile Software for Data Analysis. *Anal. Chem.* **2016**, *88* (10), 5050–5052. https://doi.org/10.1021/acs.analchem.6b00224 .
(44) Kubas, A.; Orain, C.; De Sancho, D.; Saujet, L.; Sensi, M.; Gauquelin, C.; Meynial-Salles, I.; Soucaille, P.; Bottin, H.; Baffert, C.; Fourmond, V.; Best, R. B.; Blumberger, J.; Léger, C. Mechanism of O2 Diffusion and Reduction in FeFe Hydrogenases. *Nat. Chem.* **2017**, *9* (1), 88–95. https://doi.org/10.1038/nchem.2592 .
(45) Léger, C.; Dementin, S.; Bertrand, P.; Rousset, M.; Guigliarelli, B. Inhibition and Aerobic Inactivation Kinetics of Desulfovibrio Fructosovorans NiFe Hydrogenase Studied by Protein Film Voltammetry. *J. Am. Chem. Soc.* **2004**, *126* (38), 12162–12172. https://doi.org/10.1021/ja046548d .
(46) Rodríguez-Maciá, P.; Galle, L. M.; Bjornsson, R.; Lorent, C.; Zebger, I.; Yoda, Y.; Cramer, S. P.; DeBeer, S.; Span, I.; Birrell, J. A. Caught in the Hinact : Crystal Structure and Spectroscopy Reveal a Sulfur Bound to the Active Site of an O2 -Stable State of [FeFe] Hydrogenase. *Angew. Chem. Int. Ed Engl.* **2020**, *59* (38), 16786–16794. https://doi.org/10.1002/anie.202005208 .
(47) Corrigan, P. S.; Majer, S. H.; Silakov, A. Evidence of Atypical Structural Flexibility of the Active Site Surrounding of an [FeFe] Hydrogenase from Clostridium Beijerinkii. *J. Am. Chem. Soc.* **2023**, *145* (20), 11033–11044. https://doi.org/10.1021/jacs.2c13458 .
(48) Heghmanns, M.; Rutz, A.; Kutin, Y.; Engelbrecht, V.; Winkler, M.; Happe, T.; Kasanmascheff, M. The Oxygen-Resistant [FeFe]-Hydrogenase CbA5H Harbors an Unknown Radical Signal. *Chem. Sci.* **2022**, *13* (24), 7289–7294. https://doi.org/10.1039/d2sc00385f .
(49) Richardson, J. S.; Videau, L. L.; Williams, C. J.; Richardson, D. C. Broad Analysis of Vicinal Disulfides: Occurrences, Conformations with Cis or with Trans Peptides, and Functional Roles Including Sugar Binding. *J. Mol. Biol.* **2017**, *429* (9), 1321–1335. https://doi.org/10.1016/j.jmb.2017.03.017 .
(50) Winkler, M.; Duan, J.; Rutz, A.; Felbek, C.; Scholtysek, L.; Lampret, O.; Jaenecke, J.; Apfel, U. P.; Gilardi, G.; Valetti, F.; Fourmond, V.; Hofmann, E.; Léger, C.; Happe, T. A Safety Cap Protects Hydrogenase from Oxygen Attack. *Nat. Comm. (in press, NCOMMS-20-24274B)*. 2021.
(51) Kulka-Peschke, C. J.; Schulz, A.-C.; Lorent, C.; Rippers, Y.; Wahlefeld, S.; Preissler, J.; Schulz, C.; Wiemann, C.; Bernitzky, C. C. M.; Karafoulidi-Retsou, C.; Wrathall, S. L. D.; Procacci, B.; Matsuura, H.; Greetham, G. M.; Teutloff, C.; Lauterbach, L.; Higuchi, Y.; Ishii, M.; Hunt, N. T.; Lenz, O.; Zebger, I.; Horch, M. Reversible Glutamate Coordination to High-Valent Nickel Protects the Active Site of a [NiFe] Hydrogenase from Oxygen. *J. Am. Chem. Soc.* **2022**, *144* (37), 17022–17032. https://doi.org/10.1021/jacs.2c06400 .
(52) Kumar, R.; Stein, M. The Fully Oxidized State of the Glutamate Coordinated O2-Tolerant [NiFe]-Hydrogenase Shows a Ni(III)/Fe(III) Open-Shell Singlet Ground State. *J. Am. Chem. Soc.* **2023**, *145* (20), 10954–10959. https://doi.org/10.1021/jacs.3c02438 .